A novel route to rhodaboratranes $[Rh(CO)(PR_3)\{B(taz)_3\}]^+$ *via* the redox activation of scorpionate complexes [RhLL′Tt]†

Robin J. Blagg,‡ Christopher J. Adams, Jonathan P. H. Charmant, Neil G. Connelly,* Mairi F. Haddow, Alex Hamilton, James Knight, A. Guy Orpen and Benjamin M. Ridgway

Received 22nd May 2009, Accepted 3rd August 2009
First published as an Advance Article on the web 28th August 2009
DOI: 10.1039/b910108j

The reaction of a mixture of the sodium salts of dihydrobis(4-ethyl-3-methyl-5-thioxo-1,2,4-triazolyl)-borate, NaBt, and hydrotris(4-ethyl-3-methyl-5-thioxo-1,2,4-triazolyl)borate, NaTt, with $[\{Rh(cod)(\mu\text{-}Cl)\}_2]$ gave [Rh(cod)Bt] and [Rh(cod)Tt], which separately react with CO gas to give the unstable dicarbonyl $[Rh(CO)_2Bt]$ and an equilibrium mixture of two isomers of $[Rh(CO)_2Tt]$ and $[(RhTt)_2(\mu\text{-}CO)_3]$, respectively. Tertiary phosphorus donor ligands react with the mixture of $[Rh(CO)_2Tt]$ and $[(RhTt)_2(\mu\text{-}CO)_3]$ to give $[Rh(CO)(PR_3)Tt]$ (R = Cy, NMe_2, Ph or OPh) and $[Rh\{P(OPh)_3\}_2Tt]$ in which rhodium is bound to two sulfur atoms of the scorpionate ligand; the B–H bond is directed towards the metal to give an agostic-like B–H ⋯ Rh interaction. Dinuclear $[(RhTt)_2(\mu\text{-}CO)_3]$ has $\kappa^3[S_3]$-bound Tt ligands with a rhodium–rhodium bond bridged by three carbonyls. In solution the mononuclear Tt complexes undergo rapid dynamic interchange of the three thioxotriazolyl rings, probably *via* $\kappa^3[S_3]$-coordinated intermediates. The monocarbonyls $[Rh(CO)(PR_3)Tt]$ (R = Cy, NMe_2 or Ph) react with two equivalents of $[Fe(\eta\text{-}C_5H_5)_2][PF_6]$ in the presence of triethylamine to give the monocationic rhodaboratranes $[Rh(CO)(PR_3)\{B(taz)_3\}]^+$, with boron NMR spectroscopy providing evidence for the boron–rhodium bond. In the solid state, rhodium is bound to the three sulfur atoms and the boron of the $B(taz)_3$ fragment, forming a tricyclo[3.3.3.0] cage. The phosphine is *trans* to the Rh–B bond, the long Rh–P bond indicating a pronounced *trans* influence for the coordinated boron. The cation $[Rh(CO)(PPh_3)\{B(taz)_3\}]^+$ reacts with $[NBu^n_4]I$ to give $[Rh(PPh_3)I\{B(taz)_3\}]$, in which the halide is *trans* to the Rh–B bond, and a second species, possibly $[Rh(CO)I\{B(taz)_3\}]$. The dirhodaboratrane $[Rh_2(PCy_3)\{B(taz)_3\}_2][PF_6]_2$, a minor byproduct in the synthesis of $[Rh(CO)(PCy_3)\{B(taz)_3\}][PF_6]$, has a distorted square pyramidal rhodium atom with a vacant site *trans* to the Rh–B bond. The second metal has four coordination sites filled by the sulfur and boron atoms of a second $B(taz)_3$ unit, the remaining octahedral sites occupied by two of the sulfur atoms of the first $B(taz)_3$ unit which therefore bridges the two rhodium atoms.

Introduction

The archetypal scorpionate ligands, the *N*-donor hydrotris(pyrazolyl)borates (*e.g.* Tp′, Fig. 1), have been widely used in coordination and organometallic chemistry, commonly as analogues of the cyclopentadienyl ligand.[1] However, in recent years *S*-donor scorpionates have been reported, including hydrotris(2-thio-1-methyl-imidazolyl)borate {Tm or $HB(mt)_3$}[2] and hydrotris(4-ethyl-3-methyl-5-thioxo-1,2,4-triazolyl)borate {Tt or $HB(taz)_3$}; the latter is capable of acting as an *S*- or *N*-donor depending on the metal centre.[3] In addition to the electronic effects of changing the donor atoms, there are steric differences resulting from *N*- and *S*-donation, with two atoms between the bridgehead (boron) and the bound metal for the former and three for the latter.

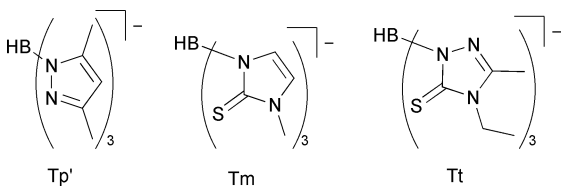

Fig. 1 The scorpionate ligands Tp′, Tm and Tt.

Rhodium(I) complexes of Tp′, *e.g.* $[RhL_2Tp']$ (Fig. 2), can adopt a variety of structures, an extensive computational investigation identifying four major isomers and the mechanism of interchange between them.[4] Two structures feature κ^3-coordination of the scorpionate, giving trigonal bipyramidal (TBP) or square pyramidal (SPY) metal centres; in these Tp′ can be viewed as analogous to a cyclopentadienyl ligand, *i.e.* an anionic, face-capping, six-electron donor. Interchange between the TBP and SPY isomers can result in exchange of the donor pyrazolyl rings through a 'reverse' Berry pseudorotation. The other structures have Tp′ coordinated through two pyrazolyl rings to a square-planar metal centre,

School of Chemistry, University of Bristol, Bristol, UK BS8 1TS. E-mail: Neil.Connelly@bristol.ac.uk; Fax: +44 (0)117 9290509; Tel: +44 (0)117 9288162

† Electronic supplementary information (ESI) available: Structures of **2**, **7**, **8**, **12**$^+$ and **13**$^+$; proton NMR data for **2** and **8** at –80 °C. CCDC reference numbers 733499–733503 and 733505–733509. For ESI and crystallographic data in CIF or other electronic format see DOI: 10.1039/b910108j

‡ Present address: Department of Chemistry and Biochemistry, University of Sussex, Falmer, Brighton, UK, BN1 9QJ. E-mail: rb250@sussex.ac.uk

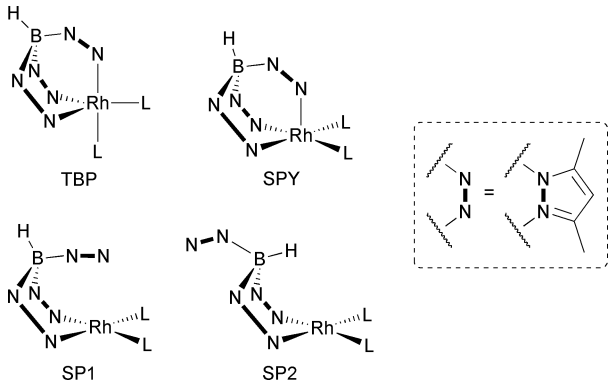

Fig. 2 Structures of [RhL$_2$Tp′].

with the uncoordinated ring either pseudo-parallel to the square plane (SP1) or directed away from the metal centre (SP2); these structures are linked by inversion of the six-membered B(NN)$_2$Rh ring.

A recent review details the wide ranging chemistry of rhodium hydrotris(pyrazolyl)borates,[5] including examples of C–H activation and of polymerisation catalysis. Studies[6] of the redox chemistry of rhodium(I) Tp′ complexes resulted in the isolation of rhodium(II) species stabilised through coordination of the third pyrazolyl ring to rhodium. In contrast, rhodium complexes of the *S*-donor ligands hydrotris(2-thio-1-R-imidazolyl)borate (R = Me, Pr^i or Bu^t), made from either rhodium(I) or rhodium(III) precursors, can undergo B–H bond activation to give octahedral rhodaboratranes (with rhodium–boron bonds).[7,8]

We have briefly reported[9] that the rhodium(I) complex [Rh(CO)(PPh$_3$)Tt] has a κ^3[S$_2$H]-coordinated scorpionate in the solid state and that two-electron oxidation gives the rhodaboratrane complex [Rh(CO)(PPh$_3$){B(taz)$_3$}]$^+$, the first to be synthesised directly from a rhodium scorpionate precursor under controlled reaction conditions. We now give details of the synthesis, characterisation and electrochemistry of a wider range of complexes of the form [RhLL′Tt], and their two-electron oxidation to yield a series of fully characterised rhodaboratranes, the reactivity of which has also been explored.

Results and discussion

The scorpionate ligand Tt was synthesised as its sodium salt by the reaction of 4-ethyl-3-methyl-5-thioxo-1,2,4-triazole, H(taz), with NaBH$_4$. Performing the reaction under the conditions previously reported[3] invariably resulted in the generation of sodium dihydrobis(thioxotriazolyl)borate, NaBt, a species indistinguishable from NaTt by either NMR spectroscopy or elemental analysis[3,10] but distinguished by negative-ion electro-spray ionisation mass spectrometry. Modification of the synthesis, by increasing the reaction temperature to 175 °C and reducing the reaction time, resulted in a solid comprising mainly of NaTt but still with 5–10% NaBt, as suggested by mass spectrometry. Further improvement of the product purity did not prove possible, and the presence of a mixture of ligands therefore had to be accounted for during the synthesis of Tt rhodium complexes.

Synthesis and characterisation of rhodium(I) (thioxotriazolyl)borate complexes

The complexes [Rh(cod)Bt] **1** and [Rh(cod)Tt] **2** were prepared by reacting [{Rh(cod)(μ-Cl)}$_2$] with a mixture of the sodium salts of the bis- and tris(thioxotriazolyl)borate scorpionates in dichloromethane for 2.5 h, before separating the two species by column chromatography and isolating the solid products. Bubbling carbon monoxide through a CH_2Cl_2 solution of **1** gave the unstable dicarbonyl [Rh(CO)$_2$Bt] **3** {ν(CO) 2067, 2002 cm^{-1}}, while the reaction of CO with **2** under the same conditions gave a mixture of three species in equilibrium: two isomers of [Rh(CO)$_2$Tt], **4a** {ν(CO) 2071, 2005 cm^{-1}} and **4b** {ν(CO) 2050, 1982 cm^{-1}}, and the carbonyl-bridged dirhodium complex [(RhTt)$_2$(μ-CO)$_3$] **5** {ν(CO) 1826 cm^{-1}}. Concentration of this solution *in vacuo* drove the equilibrium towards **5**, which was then isolable in good yield. Addition of stoichiometric amounts of tertiary phosphines to the CH_2Cl_2 solution of **4a**, **4b** and **5** gave, over 1–2 h, the complexes [Rh(CO)(PR$_3$)Tt] (R = Cy **6**, NMe$_2$ **7**, Ph **8** or OPh **9**) and [Rh{P(OPh)$_3$}$_2$Tt] **10**, which were isolated as yellow or orange solids.

Complexes **1**, **2**, **5–8** and **10** were characterised by X-ray crystallography and, with **9**, by elemental analysis, IR spectroscopy (Table 1) and ^{1}H, ^{13}C-{^{1}H}, ^{31}P-{^{1}H} and ^{11}B-{^{1}H} NMR spectroscopy (Table 2). Cyclic voltammetry has been used to probe the redox processes of the Tt complexes **2** and **6–10**.

The carbonyl stretching frequencies of **6–9** vary in accordance with Tolman's electronic parameter for phosphine ligands,[11] as also observed for their Tp′ analogues.[6] The two isomers of [Rh(CO)$_2$Tt] **4** observed by IR spectroscopy are proposed to involve different coordination modes of the Tt ligand, *i.e.* coordination of either two

Table 1 Analytical and IR spectroscopic data for [Rh(cod)Bt] **1**, [RhLL′Tt] **2**, **6–10** and [(RhTt)$_2$(μ-CO)$_3$}] **5**

Complex	Colour	Yield (%)	Analysis (%)[a] C	H	N	ν(CO)/cm^{-1}
[Rh(cod)Bt] **1**	Yellow	6	42.2 (42.5)	5.8 (5.9)	16.2 (16.5)	—
[Rh(cod)Tt] **2**	Yellow-orange	33	42.3 (42.5)	5.9 (5.7)	19.1 (19.4)	—
[(RhTt)$_2$(μ-CO)$_3$}] **5**	Yellow-brown	84	33.9 (34.0)	4.4 (4.3)	21.8 (21.6)	1826
[Rh(CO)(PCy$_3$)Tt] **6**	Yellow	61	48.2 (48.1)	7.0 (6.9)	14.9 (14.8)	1956
[Rh(CO){P(NMe$_2$)$_3$}Tt] **7**	Yellow-orange	65	34.0 (33.8)[b]	5.4 (5.5)	20.5 (20.6)	1968
[Rh(CO)(PPh$_3$)Tt] **8**	Yellow	75	46.1 (45.9)[b]	4.5 (4.6)	13.7 (13.8)	1977
[Rh(CO){P(OPh)$_3$}Tt] **9**	Yellow-orange	40	46.2 (46.4)	4.4 (4.6)	14.4 (14.3)	2004
[Rh{P(OPh)$_3$}$_2$Tt] **10**	Yellow	65	53.0 (52.7)	4.7 (4.8)	10.5 (10.8)	—

[a] Calculated values in parentheses. [b] Calculated as a 1 : 1 CH_2Cl_2 solvate.

Table 2 Proton, ^{13}C-{^{1}H}, ^{31}P-{^{1}H} and ^{11}B-{^{1}H} NMR spectroscopic data for [Rh(cod)Bt] **1**, [RhLL′Tt] **2**, **6–10** and [(RhTt)$_2$(μ-CO)$_3$}] **5**[a]

Complex	^{1}H	^{13}C-{^{1}H}	^{31}P-{^{1}H}	^{11}B-{^{1}H}
[Rh(cod)Bt] **1**	4.03 (br s, 4H, cod C*H*), 3.87 (q, 4H, $^{3}J_{HH}$ 7.2, Bt 4-CH_2CH$_3$), 2.46–2.30 (br m, 4H, cod CH_2), 2.25 (s, 6H, Bt 3-CH_3), 1.79 (q, 4H, J_{HH} 8.2, cod CH_2), 1.19 (t, 6H, $^{3}J_{HH}$ 7.2, Bt 4-CH$_2$CH_3)[b]	165.90 (s, Bt C^5), 149.14 (s, Bt C^3), 78.99 (d, $^{1}J_{CRh}$ 12.3, cod *C*H), 39.83 (s, Bt 4-*C*H$_2$CH$_2$), 31.82 (s, cod *C*H$_2$), 13.71 (s, Bt 3-*C*H$_3$), 11.11 (s, Bt 4-CH$_2$*C*H$_3$)[b]	—	−7.93 (s, Bt *B*H$_2$)[b]
[Rh(cod)Tt] **2**	4.27 (br s, 4H, cod C*H*), 4.01 (q, 6H, $^{3}J_{HH}$ 7.0, Tt 4-CH_2CH$_3$), 2.60–2.46 (br m, 4H, cod CH_2), 2.33 (s, 9H, Tt 3-CH_3), 1.81 (q, 4H, J_{HH} 8.1, cod CH_2), 1.28 (t, 9H, $^{3}J_{HH}$ 7.0, Tt 4-CH$_2$CH_3)	148.61 (s, Tt C^3), 80.99 (d, $^{1}J_{CRh}$ 10.9, cod *C*H), 39.88 (s, Tt 4-*C*H$_2$CH$_2$), 31.99 (s, cod *C*H$_2$), 13.96 (s, Tt 3-*C*H$_3$), 11.67 (s, Tt 4-CH$_2$*C*H$_3$)	—	−5.24 (s, Tt *B*H)
[Rh(CO)(PCy$_3$)Tt] **6**	4.06 (q, 6H, $^{3}J_{HH}$ 7.2, Tt 4-CH_2CH$_3$), 2.35 (s, 9H, Tt 3-CH_3), 2.18-1.51 (br m, 33H, P*Cy*$_3$), 1.32 (t, 6H, $^{3}J_{HH}$ 7.2, Tt 4-CH$_2$CH_3)	167.36 (s, Tt C^3), 28.66–26.36 (m, P*Cy*$_3$), 14.24 (s, Tt 3-*C*H$_3$), 11.87 (s, Tt 4-CH$_2$*C*H$_3$)	50.63 (d, $^{1}J_{PRh}$ 155, *P*Cy$_3$)	−5.17 (s, Tt *B*H)
[Rh(CO){P(NMe$_2$)$_3$}Tt] **7**	4.05 (q, 6H, $^{3}J_{HH}$ 7.3, Tt 4-CH_2CH$_3$), 2.74 {d, 18H, $^{3}J_{HP}$ 10.6, P(N*Me*$_2$)$_3$}, 2.35 (s, 9H, Tt 3-CH_3), 1.31 (t, 6H, $^{3}J_{HH}$ 7.3, Tt 4-CH$_2$CH_3)	148.74 (s, Tt C^3), 39.84 (s, Tt 4-*C*H$_2$CH$_2$), 39.33 {d, $^{2}J_{CP}$ 6.3, P(N*Me*$_2$)$_3$}, 14.05 (s, Tt 3-*C*H$_3$), 11.73 (s, Tt 4-CH$_2$*C*H$_3$)	126.14 {d, $^{1}J_{PRh}$ 207, *P*(NMe$_2$)$_3$}	−5.37 (s, Tt *B*H)
[Rh(CO)(PPh$_3$)Tt] **8**	7.84–7.29 (m, 15H, P*Ph*$_3$), 3.88 (br q, 6H, $^{3}J_{HH}$ 7.1, Tt 4-CH_2CH$_3$), 2.31 (s, 9H, Tt 3-CH_3), 1.21 (t, 9H, $^{3}J_{HH}$ 7.1, Tt 4-CH$_2$CH_3)	148.76 (s, Tt C^3), 134.55 (d, J_{CP} 12.9, P*Ph*$_3$), 130.15 (d, J_{CP} 2.3, P*Ph*$_3$), 128.37 (d, J_{CP} 10.4, P*Ph*$_3$), 39.89 (s, Tt 4-*C*H$_2$CH$_2$), 13.99 (s, Tt 3-*C*H$_3$), 11.67 (s, Tt 4-CH$_2$*C*H$_3$)	40.79 (d, $^{1}J_{PRh}$ 158, *P*Ph$_3$)	−4.95 (s, Tt *B*H)
[Rh(CO){P(OPh$_3$}Tt] **9**	7.38–7.10 {m, 15H, P(O*Ph*$_3$}, 3.93 (q, 6H, $^{3}J_{HH}$ 7.2, Tt 4-CH_2CH$_3$), 2.30 (s, 9H, Tt 3-CH_3), 1.21 (t, 9H, $^{3}J_{HH}$ 7.2, Tt 4-CH$_2$CH_3)	149.09 (s, Tt C^3), 129.95 {s, P(O*Ph*$_3$}, 125.05 {s, P(O*Ph*$_3$}, 121.48 {d, J_{CP} 5.8, P(O*Ph*$_3$}, 39.83 (s, Tt 4-*C*H$_2$CH$_2$), 14.09 (s, Tt 3-*C*H$_3$), 11.67 (s, Tt 4-CH$_2$*C*H$_3$)	118.44 {d, $^{1}J_{PRh}$ 272, *P*(OPh$_3$}	−4.78 (s, Tt *B*H)
[Rh{P(OPh$_3$}$_2$Tt] **10**	7.28–7.17 {m, 30H, P(O*Ph*$_3$}, 3.81 (br s, 6H, Tt 4-CH_2CH$_3$), 2.15 (s, 9H, Tt 3-CH_3), 1.10 (br t, 9H, $^{3}J_{HH}$ 7.0, Tt 4-CH$_2$CH_3)	152.24 (s, Tt C^3), 129.70 {s, P(O*Ph*$_3$}, 124.18 {s, P(O*Ph*$_3$}, 121.26 {d, J_{CP} 2.9, P(O*Ph*$_3$}, 39.74 (s, Tt 4-*C*H$_2$CH$_2$), 13.97 (s, Tt 3-*C*H$_3$), 11.50 (s, Tt 4-CH$_2$*C*H$_3$)	115.36 {d, $^{1}J_{PRh}$ 284, *P*(OPh$_3$}	−5.95 (s, Tt *B*H)
[(RhTt)$_2$(μ-CO)$_3$}] **5**	4.30 (dq, 6H, $^{2}J_{HH}$ 14.2, $^{3}J_{HH}$ 7.0, Tt 4-C*H*HCH$_3$), 3.90 (dq, 6H, $^{2}J_{HH}$ 14.2, $^{3}J_{HH}$ 7.0, Tt 4-CH*H*CH$_3$), 2.41 (s, 18H, Tt 3-CH_3), 1.29 (t, 18H, $^{3}J_{HH}$ 7.0, Tt 4-CH$_2$CH_3)	166.19 (s, Tt C^5), 149.94 (s, Tt C^3), 39.73 (s, Tt 4-*C*H$_2$CH$_2$), 14.54 (s, Tt 3-*C*H$_3$), 11.67 (s, Tt 4-CH$_2$*C*H$_3$)	—	−2.46 (br s, Tt *B*H)

[a] Chemical shift (δ) in ppm, J values in Hz; spectra recorded in CD_2Cl_2 at 20 °C unless otherwise stated. [b] In $CDCl_3$.

or three thioxotriazolyl rings to rhodium (**4a** and **4b** respectively). A comparison with ν(CO) values calculated for various isomers of [Rh(CO)$_2$Tp′][4] suggests that **4a** has an SP1 or SP2 structure while **4b** has an SPY-type structure. The ν(BH) absorbances, measurement of which might have assisted assignment of the scorpionate bonding mode, were not observed in solution or the solid state for any of these species.

Structures of complexes 1, 2, 5–8 and 10

The molecular structures of **1**, **2**, **5–8** and **10** were determined by X-ray crystallography (Table 3). In each case, crystals were grown by allowing *n*-hexane to diffuse slowly into a concentrated CH_2Cl_2 solution of the complex at *ca.* −10 °C.

The rhodium atom of the Bt complex **1** (Fig. 3) is bound to the scorpionate ligand through the two sulfur atoms, and to the cod ligand by the two alkene bonds. One of the B–H bonds is directed towards the rhodium centre, leading to an agostic-like B–H···Rh interaction, as also observed for the related complex [Rh(cod){H$_2$B(mt)$_2$}], which was described as having a three-centre–two-electron B–H···Rh bond.[12]

The Tt complexes **2** (Fig. 4) and **6–8** (see Fig. 5 for **6** as a representative example) adopt broadly similar geometries in the solid state. As in **1**, the rhodium atom is bound in a plane to a

Table 3 Selected bond lengths (Å) and angles (°) for [Rh(cod)Bt] and [RhLL′Tt]

	[Rh(cod)Bt] **1**	[Rh(cod)Tt] **2**[a]	[Rh(CO)(PCy$_3$)-Tt] **6**	[Rh(CO){P(NMe$_2$)$_3$}-Tt] **7**	[Rh(CO)(PPh$_3$)-Tt] **8**[b]	[Rh{P(OPh)$_3$}$_2$-Tt] **10**
Rh(1)–X(1)[c]	2.006	2.009, 2.017	1.822(7)	1.823(5)	1.817(3)	2.181(3)
Rh(1)–X(2)[d]	2.040	2.003, 2.005	2.239(2)	2.251(1)	2.264(1)	2.188(2)
Rh(1)–S(1)	2.443(1)	2.462(1), 2.372(1)	2.421(2)	2.393(1)	2.431(1)	2.401(2)
Rh(1)–S(2)	2.375(1)	2.380(1), 2.445(1)	2.385(2)	2.458(1)	2.414(1)	2.395(2)
Rh(1)···S(3)	—	4.709, 4.953	5.001	4.998	5.236	5.856
Rh(1)···B(1)	3.115	3.233, 3.120	3.362	3.465	3.239	3.995
C(1)–O(1)	—	—	1.152(8)	1.122(7)	1.152(4)	—
B(1)–N(1)	1.552(3)	1.544(6), 1.534(6)	1.553(9)	1.561(5)	1.542(5)	1.593(10)
B(1)–N(4)	1.550(3)	1.548(6), 1.541(6)	1.550(10)	1.557(10)	1.537(5)	1.560(10)
B(1)–N(7)		1.518(6), 1.544(6)	1.531(10)	1.530(6)	1.536(5)	1.522(11)
S(1)–Rh(1)–S(2)	95.34(3)	95.71(4), 94.40(5)	95.38(8)	95.18(4)	93.62(4)	96.10(8)
X(1)–Rh(1)–X(2)	87.02	87.61, 87.17	88.6(2)	86.33(16)	90.11(12)	90.19(9)
S(1)–Rh(1)–X(1)	158.02	170.52, 169.78	1.778(2)	174.95(15)	162.59(12)	171.04(8)
S(2)–Rh(1)–X(2)	173.22	171.59, 163.12	164.14(7)	166.18(4)	168.86(3)	161.51(8)
N(1)–B(1)···Rh(1)–S(1)	15.24	–31.66, –11.77	–20.68	32.91	26.48	39.93
N(4)–B(1)···Rh(1)–S(2)	5.62	–29.82, –19.62	–23.98	31.87	20.39	28.64
N(7)–B(1)–Rh(1)–S(3)	—	–13.22, –49.21	–42.53	22.19	49.88	15.38
S(3)–N(7)–B(1)···Rh(1)	—	16.43, 66.10	54.19	–27.38	–68.30	–18.36

[a] Two distinct molecules in the unit cell. [b] Data from reference 9. [c] X(1): **1**, midpoint of C(12)–C(13); **2**, midpoint of C(17)–C(18); **6–8**, C(1); **10**, P(1). [d] X(2): **1**, midpoint of C(16)–C(17); **2**, midpoint of C(21)–C(22); **6–8**, P(1); **10**, P(2).

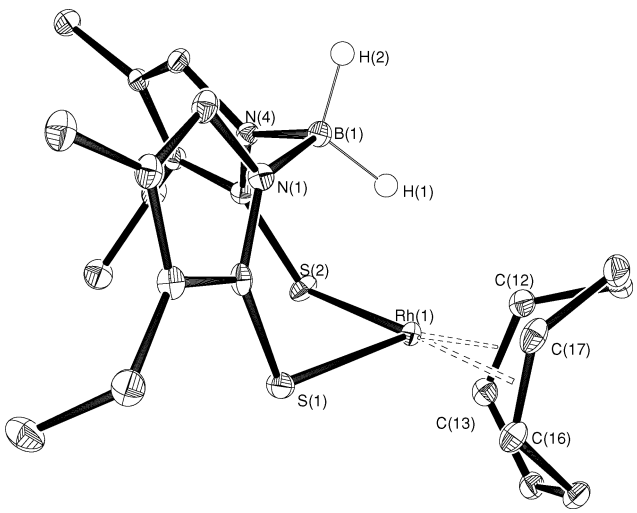

Fig. 3 Molecular structure of [Rh(cod)Bt] **1**. (In this structure, and all others in this paper, ellipsoids are shown at the 50% probability level; most hydrogen atoms are omitted for clarity.)

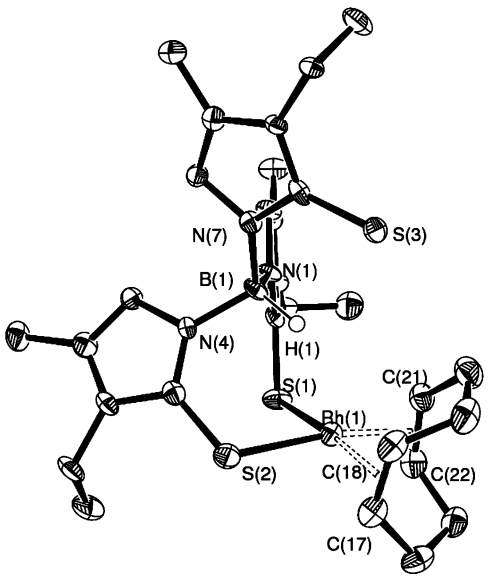

Fig. 4 Molecular structure of [Rh(cod)Tt] **2**. (Only one of the two distinct molecules in the unit cell is shown.)

sulfur atom of each of two thioxotriazolyl rings and to the ancillary ligand(s), either cod or CO and PR$_3$. The Tt scorpionate has the uncoordinated thioxotriazolyl ring directed away from, and the B–H bond directed towards, the rhodium centre. By analogy with their Tp analogues, these structures can be described as SP2-type (Fig. 2).

The unit cell of **2** contains two independent but broadly similar molecules. Though there are negligible differences in the rhodium coordination sphere, the scorpionate ligands of the two molecules have different conformations, specifically involving the orientation of the uncoordinated thioxotriazolyl ring. Rotation about the B(1)–N(7) bond leads to different positioning of the uncoordinated sulfur atom, shown by the dihedral angles S(3)–N(7)–B(1)···Rh(1) (16.5 and 66.1° for the two molecules).

The bis(phosphite) complex **10** (Fig. 6) has, as with **2** and **6–8**, an SP2-type structure with the approximately square planar rhodium centre bound to two sulfur atoms and the two P(OPh)$_3$ ligands. However, both phosphite ligands are displaced from the idealised square plane to minimise steric interference; P(1) is raised by 0.25 Å above the plane defined by Rh(1), S(1) and S(2) but P(2) is 0.69 Å below the plane. (Similar distortions involving the two phosphorus ligands of the rhodium(II) scorpionates [Rh(PPh$_3$)$_2$L]$^+$ {L = Tp, Tp′ or B(pz)$_4$} result in ESR spectra showing coupling of the unpaired electron to only one phosphorus nucleus.[6]) In addition, the conformation of the scorpionate results in the B–H bond being nearly parallel to the rhodium square plane, in a

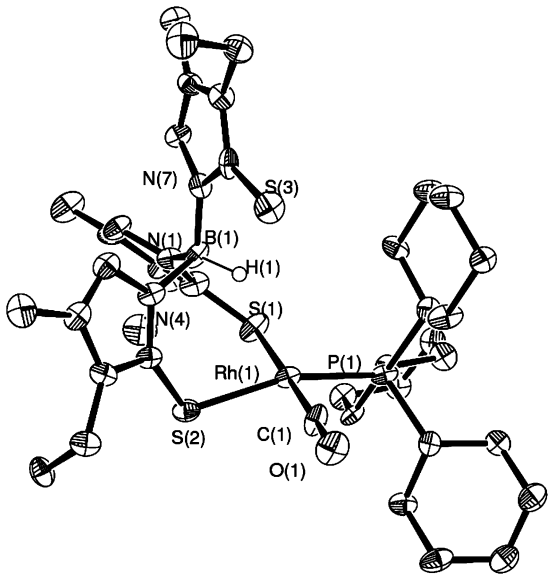

Fig. 5 Molecular structure of [Rh(CO)(PCy$_3$)Tt] **6**.

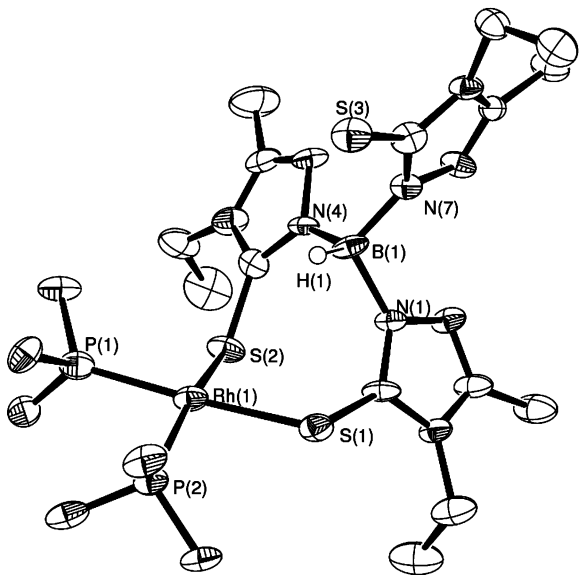

Fig. 6 Molecular structure of [Rh{P(OPh)$_3$}$_2$Tt] **10**. (The phenyl rings are omitted for clarity.)

greater Rh · · · B distance (*ca.* 4.0 Å) than in the other Tt complexes (3.1–3.5 Å), and in a reduced B–H · · · Rh interaction.

The molecular structure of [(RhTt)$_2$(μ-CO)$_3$] **5** (Fig. 7, Table 4) is nearly D_{3h} symmetric, with the Tt ligands κ^3[S$_3$]-coordinated to two rhodium atoms which are linked by a metal–metal bond and bridged by three carbonyls. The same crystallographically characterised Rh(μ-CO)$_3$Rh units are found in [{MeGa(pz)$_3$Rh}$_2$(μ-CO)$_3$][13] and [(CpCo{P(OEt)$_2$O}$_3$Rh)$_2$(μ-CO)$_3$].[14]

NMR spectroscopy and fluxional behaviour

In solution, the two thioxotriazolyl rings of [Rh(cod)Bt] **1** are equivalent, as observed in the solid state; the ^{1}H NMR spectrum shows six distinct proton resonances, three for cod and three for the thioxotriazolyl rings; the BH$_2$ protons are not observed. The ^{13}C NMR spectrum shows all seven carbon environments and the

Table 4 Selected bond lengths (Å) and angles (°) for [(RhTt)$_2$(μ-CO)$_3$] **5**

Rh(1)–Rh(1′)	2.560(1)
Rh(1)–S(1)	2.481(1)
Rh(1)–C(1)	2.019(5)
C(1)–O(1)	1.161(7)
B(1)-N(1)	1.542(4)
Rh(1) · · · B(1)	4.063
S(1)–Rh(1)–S(1′)	95.60(3)
C(1)–Rh(1)–C(1′)	84.11(17)
S(1)–Rh(1)–C(1)	87.15(8)
S(1)–Rh(1)–C(1′)	92.71(8)
S(1)–Rh(1)–C(1″)	170.95(10)
Rh(1)–C(1)–O(1)	140.67(11)
N(1)–B(1) · · · Rh(1)–S(1)	46.00

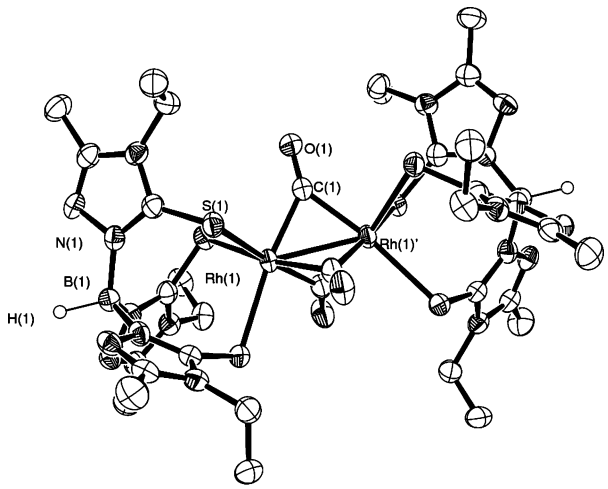

Fig. 7 Molecular structure of [(RhTt)$_2$(μ-CO)$_3$] **5**.

proton-decoupled ^{11}B NMR spectrum shows a single resonance at *ca.* δ_B −8 ppm, broadened in the proton-coupled ^{11}B NMR spectrum.

The Tt complexes **2** and **6–10** display the same general features in their room temperature NMR spectra, with the three thioxotriazolyl rings equivalent. Throughout, the BH resonances are not observed. Proton-decoupled boron spectra show single resonances at *ca.* δ_B −5 ppm, and the phosphorus spectra for the carbonyl phosphines **6–9** are consistent with those of their Tp′ analogues.[6] The ^{31}P NMR spectrum of the bis(phosphite) **10** shows δ_P (115.4 ppm) lower by *ca.* 3 ppm, and $^1J_{PRh}$ (284 Hz) larger, than for the carbonyl phosphite **9** (118.4 ppm and 272 Hz respectively).

At *ca.* −80 °C the three thioxotriazolyl rings of the Tt ligand of **2** and **6–10** are no longer equivalent on the NMR spectroscopic timescale, as previously observed for their hydrotris(pyrazolyl)borate analogues;[6,15] two (for **2** and **10**) or three (for **6–9**) thioxotriazolyl ring environments are observed in the ^{1}H NMR spectra, corresponding to the different environments observed in the solid state.

For **2** (Fig. 8), signals corresponding to the uncoordinated thioxotriazolyl ring are at a higher chemical shift than those of the coordinated rings, by *ca.* 0.1 ppm. The two methylene protons of the ethyl groups on the coordinated rings are diastereotopic, appearing as two doublets of quartets, because of slow rotation about the N–CH$_2$ bond. The low temperature ^{1}H NMR spectrum

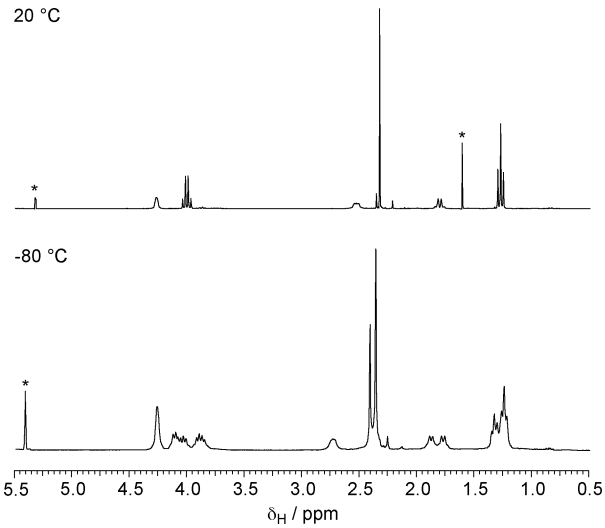

Fig. 8 Variable temperature ^{1}H NMR spectra of [Rh(cod)Tt] **2**. (Peaks marked with an asterisk are due to residual solvent/water.)

of the bis(phosphite) complex **10** is similar to that of **2** although the methyl groups of the coordinated rings show significantly lower chemical shifts than those of the uncoordinated ring ($\Delta\delta_H$ 0.3–0.4 ppm), perhaps due to shielding from the six phenyl rings surrounding the metal centre.

It is possible to assign some of the resonances in the ^{1}H NMR spectrum of **8** (Fig. 9) at −80 °C to specific thioxotriazolyl rings. By comparison with **2**, the methyl groups of the uncoordinated thioxotriazolyl ring are most probably those at 2.39 and 1.32 ppm. For each thioxotriazolyl proton environment, one set of resonances has a significantly lower chemical shift than the other two, assigned to the ring *cis* to PPh_3 due to the shielding effect of the aromatic rings, *i.e.* resonances at 3.29, 3.11, 2.21 and 0.86 ppm. The remaining methyl protons can therefore be assigned to the ring *trans* to triphenylphosphine, although the methylene protons cannot be unambiguously assigned.

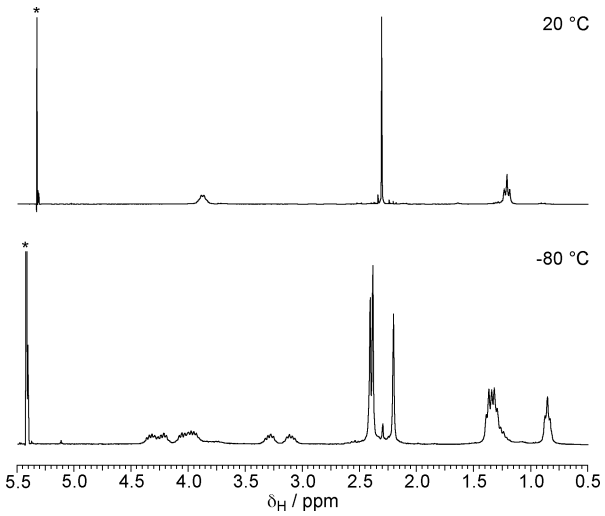

Fig. 9 Variable temperature ^{1}H NMR spectra of [Rh(CO)(PPh_3)Tt] **8** in CD_2Cl_2. (Peaks marked with an asterisk are due to residual solvent.)

Although the variable temperature NMR spectra of **6**, **7** and **9** also show three distinct thioxotriazolyl rings at low temperature, overlap of resonances renders complete assignment impossible. The carbonyl phosphite complex **9** does not show significant shielding effects on the thioxotriazolyl ring *cis* to $P(OPh)_3$ as is observed for that ring in [Rh(CO)(PPh_3)Tt] **8**; the phenyl rings of $P(OPh)_3$ in **9** are further from the metal centre than those of PPh_3 in **8**.

Overall, in solution the rhodium(I) Tt complexes undergo rapid dynamic interchange of the three thioxotriazolyl rings, possibly as shown in Scheme 1. Two square-planar isomers, SP1 and SP2, the latter observed in the solid state, are linked by inversion of the eight-membered $Rh(SCN)_2B$ ring. Coordination of the third ring would give the $\kappa^3[S_3]$-coordinated SPY isomer (as observed in solution for **4b**) from which the three thioxotriazolyl rings might undergo interchange through Berry pseudorotation *via* trigonal bipyramidal intermediates.

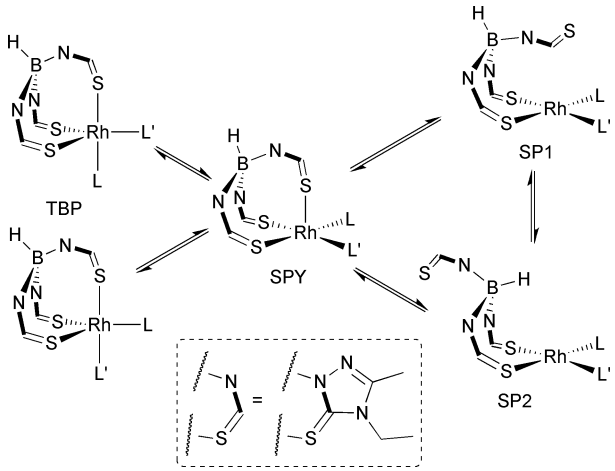

Scheme 1 Mechanism for ring-interchange in [RhLL′Tt].

Variable temperature NMR spectra of the $\kappa^3[S_3]$-coordinated, carbonyl-bridged complex **5** did not show evidence of dynamic processes, consistent with a rigid structure. The proton-decoupled boron spectrum displayed a single resonance at a more positive chemical shift than for any of the $\kappa^3[S_2H]$-coordinated ligands.

The redox chemistry of [RhLL′Tt] and the synthesis and characterisation of rhodaboratranes

Though repeatable, the cyclic voltammograms of analytically pure samples of the rhodium(I) tris(thioxotriazolyl)borate complexes **2** and **6–10** are not as well defined as those of the rhodium(I) tris(pyrazolyl)borate complexes [RhLL′Tp′].[6,15] The CVs of **2** and **6–9** are broadly similar with two irreversible oxidation waves separated by *ca.* 0.25 V; the dominant second wave has a peak potential, $(E_p)_{ox}$, of 0.39–0.49 V. An irreversible reduction wave at *ca.* 0.0–0.2 V may be linked to the first oxidation process. The CV of **10** shows only one irreversible oxidation wave, with $(E_p)_{ox}$ = 0.46 V.

The reaction of complexes **6–8** with two equivalents of the one-electron oxidant $[Fe(\eta\text{-}C_5H_5)_2][PF_6]$ in the presence of an excess of triethylamine gave, after 30 min, moderate yields of the monocationic rhodaboratrane complexes $[Rh(CO)(PR_3)\{B(taz)_3\}]^+$ (R = Cy **11**$^+$, NMe_2 **12**$^+$ or Ph **13**$^+$) as their $[PF_6]^-$ salts. These were characterised by elemental analysis, IR (Table 5), ^{1}H, ^{13}C-{^{1}H},

Table 5 Analytical and IR spectroscopic data for $[Rh(CO)(PR_3)\{B(taz)_3\}][PF_6]$

Complex	Colour	Yield (%)	Analysis (%)[a]			ν(CO)/cm^{-1}
			C	H	N	
$[Rh(CO)(PCy_3)\{B(taz)_3\}][PF_6]$ **11**$^+[PF_6]^-$	Orange	29	40.8 (41.1)	5.5 (5.8)	12.8 (12.7)	2050
$[Rh(CO)\{P(NMe_2)_3\}\{B(taz)_3\}][PF_6]$ **12**$^+[PF_6]^-$	Orange	24	30.0 (30.1)	5.0 (4.8)	19.1 (19.2)	2055
$[Rh(CO)(PPh_3)\{B(taz)_3\}][PF_6]$ **13**$^+[PF_6]^-$	Orange	26	42.1 (41.9)	4.2 (4.0)	12.9 (12.9)	2064

[a] Calculated values in parentheses.

Table 6 Proton, ^{13}C-$\{^1H\}$, ^{31}P-$\{^1H\}$ and ^{11}B-$\{^1H\}$ NMR spectroscopic data for $[Rh(CO)(PR_3)\{B(taz)_3\}][PF_6]$[a]

Complex	^1H	^{13}C-$\{^1H\}$	^{31}P-$\{^1H\}$	^{11}B-$\{^1H\}$
$[Rh(CO)(PCy_3)\{B(taz)_3\}][PF_6]$ **11**$^+[PF_6]^-$	3.92 (q, 4H, $^3J_{HH}$ 7.3, taz 4-CH_2CH$_3$), 3.88 (q, 2H, $^3J_{HH}$ 7.3, taz 4-CH_2CH$_3$), 2.46 (s, 6H, taz 3-CH_3), 2.30 (s, 3H, 3-CH_3), 2.12–1.24 (br m, 33H, PCy_3), 1.36 (t, 9H, $^3J_{HH}$ 7.3, taz 4-CH$_2$CH_3)	155.12 (br s, taz C^3), 40.50 (s, 2C, taz 4-CH_2CH$_3$), 40.38 (s, 1C, taz 4-CH_2CH$_3$), 34.11 (d, J_{CP} 9.21, PCy_3), 30.07 (s, PCy_3), 27.87 (d, J_{CP} 9.79, PCy_3), 26.62 (s, PCy_3), 14.06 (s, 2C, taz 3-CH_3), 13.94 (s, 1C, taz 3-CH_3), 11.90 (s, 2C, taz 4-CH$_2$$CH_3$), 11.82 (s, 1C, taz 4-CH$_2$$CH_3$)	17.18 (v.br s, PCy$_3$), −143.94 (septet, $^1J_{PF}$ 710, PF$_6$)	7.79 (d, $^1J_{BRh}$ 75.3, B–Rh)
$[Rh(CO)\{P(NMe_2)_3\}\{B(taz)_3\}][PF_6]$ **12**$^+[PF_6]^-$	3.91 (q, 2H, $^3J_{HH}$ 7.2, taz 4-CH_2CH$_3$), 3.90 (q, 2H, $^3J_{HH}$ 7.2, taz 4-CH_2CH$_3$), 3.88 (q, 2H, $^3J_{HH}$ 7.2, taz 4-CH_2CH$_3$), 2.69 {d, 18H, $^3J_{HP}$ 9.9, P(NMe_2)$_3$}, 2.45 (s, 6H, taz 3-CH_3), 2.30 (s, 3H, 3-CH_3), 1.35 (t, 6H, $^3J_{HH}$ 7.2, taz 4-CH$_2$CH_3), 1.12 (t, 3H, $^3J_{HH}$ 7.2, taz 4-CH$_2$CH_3)	155.12 (s, taz C^3), 39.30 (s, 2C, taz 4-CH_2CH$_3$), 39.16 (s, 1C, taz 4-CH_2CH$_3$), 37.17 {d, $^2J_{CP}$ 6.9, P(NMe_2)$_3$}, 12.88 (s, 2C, taz 3-CH_3), 12.81 (s, 1C, taz 3-CH_3), 10.73 (s, 2C, taz 4-CH$_2$$CH_3$), 10.65 (s, 1C, taz 4-CH$_2$$CH_3$)	114.13 {v.br s, P(NMe$_2$)$_3$}, −143.92 (septet, $^1J_{PF}$ 714, PF$_6$)	7.58 (d, $^1J_{BRh}$ 105.9, B–Rh)
$[Rh(CO)(PPh_3)\{B(taz)_3\}][PF_6]$ **13**$^+[PF_6]^-$	7.56–7.43 (m, 15H, PPh_3), 3.88 (q, 4H, $^3J_{HH}$ 7.4, taz 4-CH_2CH$_3$), 3.87 (q, 2H, $^3J_{HH}$ 7.4, taz 4-CH_2CH$_3$), 2.45 (s, 6H, taz 3-CH_3), 2.32 (s, 3H, 3-CH_3), 1.32 (t, 9H, $^3J_{HH}$ 7.2, taz 4-CH$_2$CH_3)	133.80 (d, J_{CP} 12.1, PPh_3), 132.47 (d, J_{CP} 29.9, PPh_3), 131.31 (br s, PPh_3), 129.55 (d, J_{CP} 9.2, PPh_3), 40.63 (s, 2C, taz 4-CH_2CH$_3$), 40.54 (s, 1C, taz 4-CH_2CH$_3$), 14.22 (s, 2C, taz 3-CH_3), 14.12 (s, 1C, taz 3-CH_3), 12.01 (s, 3C, taz 4-CH$_2$$CH_3$)	7.94 (v.br s, PPh$_3$), −143.93 (septet, $^1J_{PF}$ 714, PF$_6$)	7.52 (d, $^1J_{BRh}$ 80.0, B–Rh)

[a] Chemical shift (δ) in ppm, J values in Hz; spectra recorded in CD_2Cl_2 at 20 °C.

^{31}P-$\{^1H\}$ and ^{11}B-$\{^1H\}$ NMR spectroscopy (Table 6) and X-ray crystallography.

The IR spectra of **11**$^+$–**13**$^+$ show carbonyl bands in the range 2050–2065 cm^{-1}, compared with 1955–1980 cm^{-1} for their rhodium(I) precursors **6–8**. The large increase in ν(CO) is consistent with a decreased *d*-electron count at the metal centre. The ^1H and ^{13}C-$\{^1H\}$ NMR spectra of the rhodaboratranes **11**$^+$–**13**$^+$ show two distinct thioxotriazolyl ring environments, two mutually *trans* and one *trans* to an ancillary ligand. The ^{31}P NMR spectra showed very broad resonances for the coordinated phosphines which were not further resolved at low temperature. This broadening (half height widths *ca.* 200 Hz) is proposed to be due to the quadrupole effect of the coordinated boron nucleus, as is also observed for $[Rh(PPh_3)(CNR)\{B(mt)_3\}]^+$ and $[Rh(PR_3)(PR'_3)\{B(mt)_3\}]^+$ with half height widths of 60–300 Hz.[7] The resonances of the phosphine ligands are shifted to more negative chemical shifts ($\Delta\delta_P$ 10–30 ppm) than those of the precursors **6–8**. In the complexes $[Rh(PR_3)_2\{B(mt)_3\}]^+$ the *trans*-phosphine resonance is less positive by 20–40 ppm than for the *cis*-phosphine, a difference also observed for the *trans* and *cis* isomers of $[Rh(PPh_3)(CNR)\{B(mt)_3\}]^+$.[7]

The boron NMR spectra provide direct evidence for the presence of a boron–rhodium bond, with doublets showing $^1J_{BRh}$ between 75 and 105 Hz. Previously reported spectra for other rhodaboratranes showed only a broad singlet, with a half height width of *ca.* 50 Hz.[16]

The structures of complexes 11$^+$–13$^+$

The structures of the cationic rhodaboratranes **11**$^+$–**13**$^+$ (see Fig. 10 for **11**$^+$ as an example) were determined by X-ray crystallography (Table 7). Crystals were grown by allowing *n*-hexane to diffuse slowly into a concentrated CH_2Cl_2 solution of the $[PF_6]^-$ salt of the complex at *ca.* −10 °C. The structures are broadly similar with rhodium bound to the three sulfur atoms and the boron of the B(taz)$_3$ fragment, forming a tricyclo[3.3.3.0] cage. Of the two ancillary ligands the phosphine is *trans* to the Rh–B bond in all cases.

Table 7 Selected bond lengths (Å) and angles (°) for $[Rh(CO)(PR_3)\{B(taz)_3\}]^+$

	$[Rh(CO)(PCy_3)\{B(taz)_3\}]^+$ **11**$^+$	$[Rh(CO)\{P(NMe_2)_3\}\{B(taz)_3\}]^+$ **12**$^+$	$[Rh(CO)(PPh_3)\{B(taz)_3\}]^+$ **13**$^{+a}$
Rh(1)–B(1)	2.173(5)	2.176(2)	2.153(5)
Rh(1)–S(1)	2.402(1)	2.411(2)	2.387(1)
Rh(1)–S(2)	2.388(1)	2.372(1)	2.386(1)
Rh(1)–S(3)	2.386(1)	2.383(1)	2.397(1)
Rh(1)–P(1)	2.550(1)	2.485(1)	2.495(1)
Rh(1)–C(1)	1.892(5)	1.867(3)	1.857(5)
C(1)–O(1)	1.101(6)	1.118(3)	1.146(6)
B(1)–N(1)	1.548(7)	1.550(3)	1.546(6)
B(1)–N(4)	1.548(6)	1.545(3)	1.534(6)
B(1)–N(7)	1.535(6)	1.535(7)	1.533(6)
B(1)–Rh(1)–S(1)	87.15(15)	86.19(8)	88.01(13)
B(1)–Rh(1)–S(2)	83.75(14)	86.24(7)	84.37(13)
B(1)–Rh(1)–S(3)	84.00(14)	84.58(7)	84.14(13)
B(1)–Rh(1)–P(1)	173.08(15)	178.79(7)	176.60(13)
B(1)–Rh(1)–C(1)	87.0(2)	86.19(10)	87.10(19)
S(1)–Rh(1)–C(1)	172.87(14)	172.09(7)	175.10(15)
S(2)–Rh(1)–S(3)	166.12(4)	167.01(2)	165.19(4)
N(1)–B(1)–Rh(1)–S(1)	0.6(3)	3.37(13)	0.8(3)
N(4)–B(1)–Rh(1)–S(2)	−25.7(3)	−20.81(13)	−22.6(3)
N(7)–B(1)–Rh(1)–S(3)	22.7(3)	24.31(13)	25.4(3)

[a] Data from reference 9.

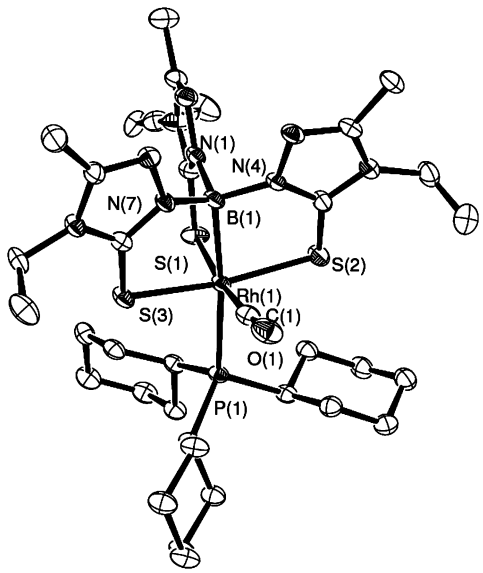

Fig. 10 Structure of the cation $[Rh(CO)(PCy_3)\{B(taz)_3\}]^+$ **11**$^+$.

The Rh–P bond lengths in the rhodaboratranes **11**$^+$–**13**$^+$ are longer than those of their rhodium(I) precursors, **6–8**, by up to 0.3 Å indicating the significant *trans* influence of the coordinated boron; the Rh–S bonds are generally somewhat shorter. The rhodium and boron coordination geometries are slightly distorted, from octahedral and tetrahedral respectively. The two *trans* thioxotriazolyl rings bridging the rhodium and boron centres are twisted {as shown by the dihedral angles N(4)–B(1)–Rh(1)–S(2) and N(7)–B(1)–Rh(1)–S(3)} to ensure the two centres optimise their preferred geometry (octahedral and tetrahedral respectively). The third ring (*cis* to the other two) shows negligible twisting {as shown by the dihedral angle N(1)–B(1)–Rh(1)–S(1), in the range 0.0–3.5°}. There is also little variation in the rigid cage structure of the $Rh(taz)_3B$ unit in **11**$^+$–**13**$^+$.

A comparison of the structures of **11**$^+$–**13**$^+$ with those of rhodaboratranes derived from Tm ligands, *e.g.* $[Rh(PPh_3)Cl\{B(mt)_3\}]$,[16] and of the ruthenaboratrane $[Ru(CO)(PPh_3)\{B(mt)_3\}]$[17] shows the rigid tricyclo[3.3.3.0] cages $B(taz)_3Rh$ and $B(mt)_3M$ to have similar bond lengths and angles. The ruthenium complex, isoelectronic with $[Rh(CO)(PPh_3)\{B(taz)_3\}]^+$ **13**$^+$, also has a long M–P bond (2.435 Å)[17] *trans* to the M–B bond, *cf*. M–P bond lengths between PPh_3 and a six-coordinate metal centre (2.321 and 2.370 Å for Rh and Ru respectively).[18] A long Rh–P bond (2.471 Å) is also observed for the phosphine *trans* to boron in $[Rh(PMe_3)_2\{B(mt)_3\}]^+$ {the *cis* bond (2.293 Å) is significantly shorter}; the cations $[Rh(PPh_3)(CNR)\{B(mt)_3\}]^+$ also have the phosphine, rather than the stronger π-acidic isocyanide CNR (isoelectronic with CO), *trans* to boron.[7]

The structure of the dirhodaboratrane $[Rh_2(PCy_3)\{B(taz)_3\}_2][PF_6]_2$ **14**$^{2+}$2$[PF_6]^-$ (Fig. 11 and Table 8) was determined from a

Table 8 Selected bond lengths (Å) and angles (°) for $[Rh_2(PCy_3)\{B(taz)_3\}_2]^{2+}$ **14**$^{2+}$

Rh(1)–P(1)	2.360(1)	B(1)–Rh(1)–S(1)	88.99(13)
Rh(1)–B(1)	2.084(5)	B(1)–Rh(1)–S(2)	87.21(14)
Rh(1)–S(1)	2.419(1)	B(1)–Rh(1)–S(3)	93.02(4)
Rh(1)–S(2)	2.384(1)	B(1)–Rh(1)–P(1)	103.27(13)
Rh(1)–S(3)	2.369(1)	B(2)–Rh(2)–S(1)	95.77(13)
Rh(2)–S(1)	2.384(1)	B(2)–Rh(2)–S(2)	173.80(14)
Rh(2)–S(2)	2.632(1)	B(2)–Rh(2)–S(4)	84.68(14)
Rh(2)–B(2)	2.098(5)	B(2)–Rh(2)–S(5)	88.52(13)
Rh(2)–S(4)	2.389(2)	B(2)–Rh(2)–S(6)	86.71(14)
Rh(2)–S(5)	2.358(1)	Rh(1)–S(1)–Rh(2)	95.21(4)
Rh(2)–S(6)	2.369(2)	Rh(1)–S(2)–Rh(2)	89.86(4)
B(1)–N(1)	1.560(6)	Rh(1)–S(1)–Rh(2)–S(2)	−13.06(3)
B(1)–N(4)	1.531(6)	Rh(2)–S(2)–Rh(1)–S(1)	−12.93(3)
B(1)–N(7)	1.390(5)	N(1)–B(1)–Rh(1)–S(1)	7.0(3)
B(2)–N(10)	1.545(6)	N(4)–B(1)–Rh(1)–S(2)	−20.6(3)
B(2)–N(13)	1.549(6)	N(7)–B(1)–Rh(1)–S(3)	33.8(3)
B(2)–N(16)	1.546(6)	N(10)–B(2)–Rh(2)–S(4)	30.6(3)
		N(13)–B(2)–Rh(2)–S(5)	6.9(3)
		N(16)–B(2)–Rh(2)–S(6)	−17.9(3)

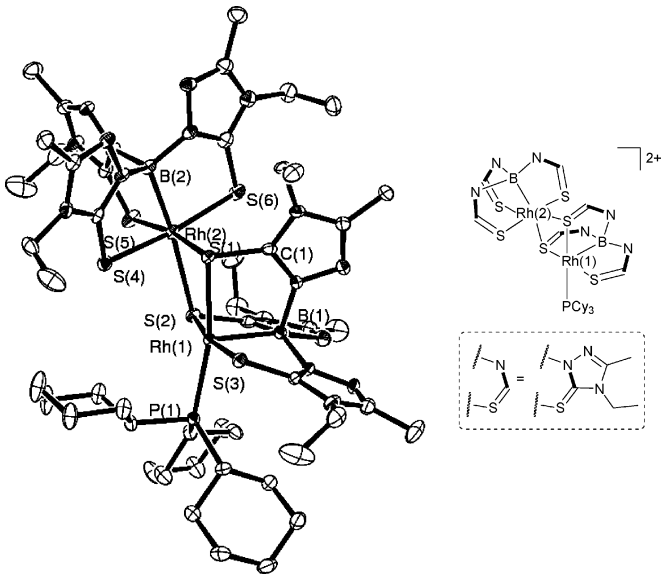

Fig. 11 Structure of the dication $[Rh_2(PCy_3)\{B(taz)_3\}_2]^{2+}$ **14**$^{2+}$.

single crystal selected from a sample of **11**$^+$[PF_6]$^-$. (The dication may therefore be a decomposition product of **11**$^+$.)

The dication **14**$^{2+}$ has one distorted square pyramidal rhodium atom, Rh(1), bound to one phosphine and the three sulfur atoms and boron of a $B(taz)_3$ unit; there is a vacant coordination site *trans* to the Rh–B bond. Space-filling models show the vacant coordination site surrounded by cyclohexyl and ethyl groups, thus providing significant steric bulk which, with the *trans* influence of the coordinated boron, deters coordination of another ligand. The second rhodium atom, Rh(2), is octahedral with four coordination sites filled by the sulfur and boron atoms of a second $B(taz)_3$ unit. The remaining two sites are occupied by two of the sulfur atoms of the first $B(taz)_3$ unit which therefore bridges the two rhodium atoms. The *trans* influence of coordinated boron is also observed in the increased length of the Rh(2)–S(2) bond {2.632(1) Å}, compared with the other rhodium–sulfur bonds present (*ca.* 2.4 Å).

The only other dirhodaboratrane complex so far reported is $[Rh_2\{B(mt)_3\}_2Tm]Cl$, obtained in low yield from the decomposition of $[Rh(PPh_3)Cl\{B(mt)_3\}]$ or by reacting $[Rh(cod)\{B(mt)_3\}]Cl$ with an excess of NaTm in $CHCl_3$ for five days.[7] The cation $[Rh_2\{B(mt)_3\}_2Tm]^+$ and **14**$^{2+}$ show similar structural features, particularly of the $[Rh_2(BR_3)_2]^{2+}$ (R = mt or taz) core unit. However, the *P*-bound and vacant sites on one rhodium of the latter are chelated by a Tm ligand in the former.

Reactions of the rhodaboratranes

In order to obtain Tt-derived rhodaboratranes which can be directly compared with known species such as $[Rh(PPh_3)Cl\{B(mt)_3\}]$,[16] stoichiometric amounts of the halide salt [NBu^n_4]I were added to dilute CH_2Cl_2 solutions of the rhodaboratrane salts **11**$^+$[PF_6]$^-$ and **13**$^+$[PF_6]$^-$. Upon completion of the reaction, as judged by IR spectroscopy, the solvent was removed *in vacuo* to give crude solid products which were analysed by IR and NMR spectroscopy.

The reaction of **13**$^+$[PF_6]$^-$ with [NBu^n_4]I over one hour resulted in the observation of a single ν(CO) band, at 2055 cm^{-1}. The ^{31}P NMR spectrum showed a single coordinated phosphine (δ_P 31.43 ppm, $^1J_{PRh}$ 120 Hz) corresponding to *ca.* 50% of the phosphorus present, the remainder accounted for as free PPh_3 and O=PPh_3. The ^{11}B-{^{1}H} NMR spectrum showed two sharp singlets at δ_B 8.15 and 7.13 ppm, *i.e.* chemical shifts in the region corresponding to rhodaboratranes. (However, the signal at 8.15 ppm may be half of a doublet, with $^1J_{BRh}$ 95 Hz, the other component of which is obscured by the more intense peak at 7.13 ppm.) The analogous reaction of **11**$^+$[PF_6]$^-$ with [NBu^n_4]I showed no apparent change in the carbonyl IR spectrum but the ^{31}P and ^{11}B NMR spectra of the solid residue showed a mixture of new species.

The crude solid obtained from the reaction of **13**$^+$[PF_6]$^-$ with [NBu^n_4]I was purified by slow diffusion of *n*-hexane into a concentrated CH_2Cl_2 solution of the product at *ca.* −10 °C, giving a mixture of orange crystals and a yellow-orange solid. X-Ray studies identified the orange crystals as the rhodaboratrane $[Rh(PPh_3)I\{B(taz)_3\}]$ **15**. The possible nature of the yellow-orange solid is briefly discussed below.

The molecular structure of $[Rh(PPh_3)I\{B(taz)_3\}]$ **15** (Fig. 12, Table 9) is very similar to that of $[Rh(PPh_3)Cl\{B(mt)_3\}]$.[16] The octahedral rhodium centre is bound to the boron and three sulfur atoms of the $B(taz)_3$ unit, giving a tricyclo[3.3.3.0] cage, along with the phosphine and halide ligands. The iodide is *trans* to the Rh–B bond with Rh(1)–I(1) (2.936(1) Å), much longer than the mean Rh–I bond distance (2.715 Å) quoted in ref. 18, reflecting the *trans* influence of the coordinated boron. Accordingly, the Rh–P bond length (Rh(1)–P(1) = 2.335(1) Å) is much closer to that in the scorpionate complex [Rh(CO)(PPh_3)Tt] **8** (2.264(1) Å) than in the boratrane $[Rh(CO)(PPh_3)\{B(taz)_3\}]^+$ **13**$^+$ (2.495(1) Å) where the phosphine is *trans* to boron.

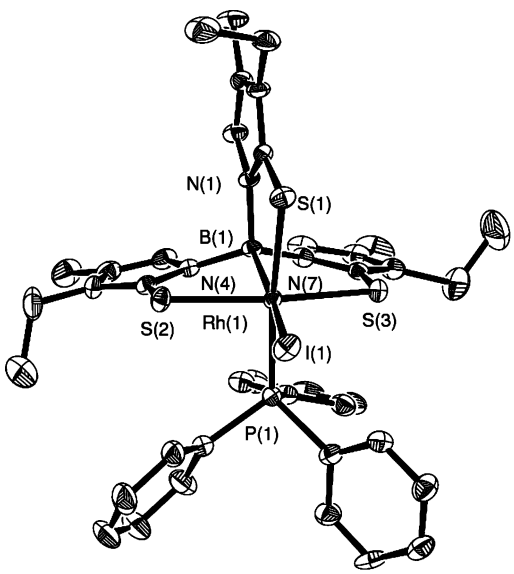

Fig. 12 Molecular structure of $[Rh(PPh_3)I\{B(taz)_3\}]$ **15**.

The IR and NMR spectra of the mixture of orange crystals and yellow-orange solid noted above showed the continued presence of two species after purification of the initial product of the reaction between $[Rh(CO)(PPh_3)\{B(taz)_3\}][PF_6]$ **13**$^+$[PF_6]$^-$ and [NBu^n_4]I. The single doublet in the ^{31}P-{^{1}H} NMR spectrum can be assigned to **15**, the absence of the quadrupole effect of the

Table 9 Selected bond lengths (Å) and angles (°) for [Rh(PPh$_3$)I{B(taz)$_3$}] **15**

Rh(1)–B(1)	2.117(5)
Rh(1)–S(1)	2.407(1)
Rh(1)–S(2)	2.372(1)
Rh(1)–S(3)	2.379(1)
Rh(1)–P(1)	2.335(1)
Rh(1)–I(1)	2.936(1)
B(1)–N(1)	1.561(6)
B(1)–N(4)	1.539(4)
B(1)–N(7)	1.527(6)
B(1)–Rh(1)–S(1)	88.18(14)
B(1)–Rh(1)–S(2)	83.49(14)
B(1)–Rh(1)–S(3)	84.79(14)
B(1)–Rh(1)–P(1)	95.53(14)
B(1)–Rh(1)–I(1)	165.29(13)
S(1)–Rh(1)–P(1)	174.73(4)
S(2)–Rh(1)–S(3)	168.12(4)
N(1)–B(1)–Rh(1)–S(1)	−3.73
N(4)–B(1)–Rh(1)–S(2)	−28.73
N(7)–B(1)–Rh(1)–S(3)	23.00

boron nucleus on the *cis*-coordinated phosphine leading to a sharp signal, in contrast to the broad resonances observed for the *trans*-coordinated phosphines in **11**$^+$–**13**$^+$. One of the two sharp singlets in the ^{11}B-{^{1}H} NMR spectrum of the mixture can also be assigned to **15**, leaving the other, and the carbonyl IR band at 2055 cm^{-1}, to be assigned to a second rhodaboratrane, reasonably assumed to be [Rh(CO)I{B(taz)$_3$}] **16**.

The mechanism of conversion of rhodium scorpionate complexes to rhodaboratranes by electron transfer, and comments on the metal–boron bond in the latter

The formation of the boratranes [Rh(CO)(PR$_3$){B(taz)$_3$}]$^+$ **11**$^+$–**13**$^+$ from the scorpionates [Rh(CO)(PR$_3$)Tt] **6–8** requires reaction with two equivalent of the one-electron oxidant [Fe(η-C$_5$H$_5$)$_2$]$^+$ in the presence of a base, *i.e.* the overall process involves the loss of two electrons and one proton. In similar redox-induced C–H activation reactions, *e.g.* where [Ru$_2$(μ-CH)(μ-CO)(μ-Ph$_2$PCH$_2$PPh$_2$)(η-C$_5$H$_5$)$_2$]$^+$ and [Mo$_2$(μ-C$_8$Me$_7$CH$_2$)(η-C$_5$H$_5$)$_2$]$^+$ are formed from [Ru$_2$(μ-CH$_2$)(μ-CO)(μ-Ph$_2$PCH$_2$PPh$_2$)(η-C$_5$H$_5$)$_2$][19] and [Mo$_2$(μ-C$_8$Me$_8$)(η-C$_5$H$_5$)$_2$][20] respectively, a mechanism involving proton loss after two-electron oxidation is supported by well-defined cyclic voltammetric studies. However, in the absence of as clearly defined voltammetry (see above), the point at which the B–H hydrogen atom is lost in the scorpionate-boratrane conversion is not known, nor whether that loss is metal-assisted, *i.e.* it is preceded by hydrogen migration from boron to rhodium. Reversible such migration is observed in, for example, the reaction of [PtH{P(C$_6$H$_4$Me-4)$_3$}{B(mt)$_3$}]$^+$ with phosphines to give [PtH(PR$_3$){B(mt)$_3$}]$^+$ *via* [Pt(PR$_3$)$_2$}{HB(mt)$_3$}]$^+$.[21]

That boratranes can be formed from scorpionates by electron transfer, at least for rhodium, has possible implications for the way in which the M–B bond in the former might be described. There has been some debate about the appropriate description of such bonds, including in Tm-derived rhodaboratranes.[22,23] Hill has proposed the notation $(M\rightarrow B)^n$ to represent the metal–boron bonding unit with, for example, [RhClL{B(mt)$_3$}]$(Rh\rightarrow B)^8$ indicating eight electrons in the rhodium non-bonding *d*-orbitals, and a two-centre–two-electron rhodium–boron dative bond.[22] However, Parkin noted that coordination of a formally Lewis acidic ligand (BR$_3$ in this case) to a metal centre results in the transfer of two electrons from a non-bonding d-orbital into the metal–boron bond, resulting in a change in the metal *d* configuration from d^n to d^{n-2}.[23] Adopting the latter approach, formal oxidation of the d^8 metal centre of **6–8** would give the d^6 octahedral rhodaboratrane complexes **11**$^+$–**13**$^+$, consistent with the need for two equivalents of a one-electron oxidant to synthesise the boratrane cations, and with the accompanying large increase in energy of ν(CO) of *ca.* 90 cm^{-1} (*e.g.* from 1956 cm^{-1} in **6** to 2050 cm^{-1} in **11**$^+$).

DFT calculations[8] on [IrCl(PH$_3$){B(mt)$_3$}] show a d^6 configuration for the metal centre {formally Ir(III), though see ref. 8 for a discussion of the relationship between *d* configuration and oxidation state in boratrane and related species} though it is interesting to note that similar calculations for [AuCl{BPh(C$_6$H$_4$PR$_2$-2)$_2$-κ^3*B*,*P*$_2$}] (R = Ph or Pr^i), coupled with ^{197}Au Mossbauer studies, showed[24] a d^{10} [Au(I)] configuration.

In both DFT studies, analysis of the frontier orbitals revealed a three-centre B–M–Cl interaction, *i.e.* the metal–boron is part of a three-centre–four-electron (3c–4e) bond also involving the *trans* ligand. These two examples appear to represent the extremes with respect to the electron distribution within an M–B bond of a boratrane and, not unexpectedly, suggest that this distribution depends on the metal and its ancillary ligands. In the end, one might argue that a definitive description of the M–B bond is less important than the chemistry which novel boratrane and related species might undergo though, of course, a more detailed understanding should eventually lead to more systematic synthetic applications.

Conclusions

The hydrotris(4-ethyl-3-methyl-5-thioxo-1,2,4-triazolyl)borate (Tt) ligands of [Rh(CO)(PR$_3$)Tt] (R = Cy, NMe$_2$, Ph or OPh) are κ^2[S$_2$]-bound in the solid state with the B–H bond part of an agostic-like B–H···Rh interaction. In solution the three thioxotriazolyl rings undergo rapid exchange at room temperature, probably *via* κ^3[S$_3$]-coordinated intermediates and Berry pseudorotation.

With two equivalents of [Fe(η-C$_5$H$_5$)$_2$][PF$_6$] in the presence of triethylamine [Rh(CO)(PR$_3$)Tt] (R = Cy, NMe$_2$ or Ph) give the monocationic rhodaboratranes [Rh(CO)(PR$_3$){B(taz)$_3$}]$^+$ in which three sulfur atoms and the boron of the B(taz)$_3$ fragment, form a tricyclo[3.3.3.0] cage with the metal. The long Rh–P bond *trans* to the coordinated boron indicates a pronounced *trans* influence which also results in a longer Rh–S bond *trans* to boron in the dirhodaboratrane [Rh$_2$(PCy$_3$){B(taz)$_3$}$_2$]$^{2+}$.

Experimental

The preparation, purification and reactions of the complexes described were carried out using Schlenk techniques under an atmosphere of dry nitrogen, using solvents dried by Anhydrous Engineering double alumina or alumina/copper catalyst columns and deoxygenated prior to use. Unless stated otherwise, complexes are stable under nitrogen and dissolve in polar solvents such as CH$_2$Cl$_2$ and thf to give air-sensitive solutions. The compounds

[{Rh(cod)(μ-Cl)}$_2$],[25] H(taz)[3] and [Fe(η-C_5H_5)$_2$][PF_6][26] were prepared by published methods. A mixture of the compounds NaBt and NaTt was prepared by a modification of the literature procedure.[3]

Solution IR spectra in CH_2Cl_2 were recorded on a Perkin Elmer Spectrum One FT-IR spectrometer. NMR spectra were recorded on a JEOL Eclipse 300 spectrometer, operating at 299.9 MHz for ^{1}H, at 75.4 MHz for ^{13}C, at 96.2 MHz for ^{11}B and at 121.4 MHz for ^{31}P, using JEOL Delta software. For ^{1}H and ^{13}C-{^{1}H} spectra, either $SiMe_4$ or residual protio solvent was used as an internal standard. For ^{31}P-{^{1}H} spectra, 85% H_3PO_4 was used as an external standard. For ^{11}B-{^{1}H} spectra, BF_3·OEt_2 was used as an external standard. Electrochemical studies were carried out using an EG&G model 273A potentiostat linked to a computer using either EG&G Model 270 Research Electrochemistry software or PAR Power Suite software, in conjunction with a three-electrode cell. The working electrode was a glassy carbon disc (3.0 mm diameter) and the counter-electrode a platinum wire. The reference was an aqueous saturated calomel electrode separated from the test solution by a fine porosity frit and an agar bridge saturated with KCl. Solutions in CH_2Cl_2 were 1.0×10^{-3} mol dm^{-3} in the test compound and 0.1 mol dm^{-3} in [NBu^n_4][PF_6] as the supporting electrolyte. Under the conditions used, $E^{\circ\prime}$ for the one-electron oxidation of [Fe(η-C_5H_4COMe)(η-C_5H_5)] or [Fe(η-C_5Me_5)$_2$], added to the test solutions as an internal calibrant is 0.74 and –0.08 V, respectively.

Microanalyses were carried out by the staff of the Microanalytical Service of the School of Chemistry, University of Bristol.

Syntheses

NaBt and NaTt. A mixture of H(taz) (3.93 g, 27.5 mmol) and $NaBH_4$ (331 mg, 8.75 mmol) was heated to *ca.* 175 °C for 3 h; hydrogen gas was evolved above 130 °C. The white solid product was cooled to room temperature, washed in a Soxhlet apparatus with hot chloroform for 6 h, then dried *in vacuo*, to give 3.13 g of a mixture comprising 90–95% NaTt and 5–10% NaBt.

[Rh(cod)Bt] 1 and [Rh(cod)Tt] 2. A solid mixture of NaBt and NaTt (1.831 g) was added to a yellow solution of [{Rh(cod)(μ-Cl)}$_2$] (944 mg, 1.91 mmol) in CH_2Cl_2 (50 cm^3). The mixture was stirred for 2.5 h then filtered through Celite, giving an orange solution which was concentrated *in vacuo* to *ca.* 5 cm^3. The concentrate was loaded onto an activated (grade III) alumina/CH_2Cl_2 chromatography column. Using CH_2Cl_2 as the mobile phase, yellow and orange-red bands separated. The first yellow band was eluted as a yellow CH_2Cl_2 solution; the second orange-red band was eluted as an orange CH_2Cl_2 : thf (3 : 1) solution. For each solution, the solvent was removed *in vacuo* and the residue redissolved in a minimum volume of CH_2Cl_2. The solution was then filtered, treated with *n*-hexane and cooled to –10 °C. The precipitated product was isolated by filtration and dried *in vacuo*. Complex **1** was obtained from the first band as a yellow solid, yield 120 mg (6%, based on rhodium) and complex **2** from the second band as a yellow-orange solid, yield 821 mg (33%, based on rhodium).§

§ Low yields are partially accounted for by adsorption of the product onto the alumina of the chromatography column.

[Rh(CO)(PCy_3)Tt] 6. Carbon monoxide was bubbled through a solution of **2** (154 mg, 181 μmol) in CH_2Cl_2 (50 cm^3) for 15 min. The phosphine PCy_3 (60 mg, 214 μmol) was then added and the mixture stirred for a further 60 min. Rapid addition of *n*-hexane and concentration of the mixture *in vacuo* gave a yellow-orange solid, isolated by filtration. The crude solid was redissolved in CH_2Cl_2 then filtered, treated with *n*-hexane and cooled to –10 °C. The precipitate was isolated by filtration and dried *in vacuo* to give a yellow solid, yield 121 mg (61%).

The complexes [Rh(CO){$P(NMe_2)_3$}Tt] **7**, [Rh(CO)(PPh_3)Tt] **8** and [Rh(CO){$P(OPh)_3$}Tt] **9** were prepared similarly.

[Rh{$P(OPh)_3$}$_2$Tt] 10. Carbon monoxide was bubbled through a solution of **2** (89 mg, 137 μmol) in CH_2Cl_2 (30 cm^3) for 15 min. An excess (*ca.* 0.1 cm^3) of $P(OPh)_3$ was then added and the reaction mixture stirred for a further 75 min. Evaporation of the mixture to dryness gave a yellow-orange solid. The crude solid was redissolved in CH_2Cl_2 then filtered, treated with *n*-hexane and cooled to –10 °C. The precipitate was isolated by filtration and dried *in vacuo* to give a yellow solid, yield 104 mg (65%).

[(RhTt)$_2$(μ-CO)$_3$] 5. Carbon monoxide was bubbled through a solution of **2** (152 mg, 234 μmol) in CH_2Cl_2 (25 cm^3) for 30 min. The solvent was then removed *in vacuo*, giving a yellow-brown solid. The crude solid was redissolved in CH_2Cl_2 then filtered, treated with *n*-hexane and cooled to –10 °C. The precipitate was isolated by filtration and dried *in vacuo* to give a yellow-brown solid, yield 114 mg (84%). All manipulations of this light-sensitive complex were carried out in the absence of light.

[Rh(CO)(PCy_3){$B(taz)_3$}][PF_6] $11^+[PF_6]^-$. To a stirred solution of **6** (101 mg, 119 μmol) in CH_2Cl_2 (65 cm^3) was added *ca.* 0.1 cm^3 triethylamine and [Fe(η-C_5H_5)$_2$][PF_6] (79 mg, 239 μmol). After 20 min the solvent was removed *in vacuo* and the crude product washed with 3 × 20 cm^3 portions of *n*-hexane and then dried *in vacuo*. The solid was dissolved in *ca.* 2 cm^3 CH_2Cl_2 and filtered through a short activated (grade III) alumina/CH_2Cl_2 chromatography column. A yellow CH_2Cl_2 solution was eluted which was concentrated *in vacuo* to *ca.* 5 cm^3. Addition of *n*-hexane to the concentrate and cooling the mixture to –10 °C gave an orange solid which was dried *in vacuo*, yield 34 mg (29%).‡

The compounds [Rh(CO){$P(NMe_2)_3$}{$B(taz)_3$}][PF_6] $\mathbf{12}^+[PF_6]^-$ and [Rh(CO)(PPh_3){$B(taz)_3$}][PF_6] $\mathbf{13}^+[PF_6]^-$ were prepared similarly, from **7** and **8** respectively.

Structure determinations

Many of the details of the structure analyses of [Rh(cod)Bt] **1**, [Rh(cod)Tt]·0.5H_2O **2**·0.5H_2O, [(RhTt)$_2$(μ-CO)$_3$] **5**, [Rh(CO)(PCy_3)Tt]·CH_2Cl_2 **6**·CH_2Cl_2, [Rh(CO)(PPh_3)Tt]·CH_2Cl_2 **8**·CH_2Cl_2, [Rh{$P(OPh)_3$}$_2$Tt]·1.5CH_2Cl_2 **10**·2CH_2Cl_2, [Rh(CO)-{$P(NMe_2)_3$}{$B(taz)_3$}][PF_6] $\mathbf{12}^+[PF_6]^-$, [Rh(CO)(PPh_3){$B(taz)_3$}]-[PF_6]·2CH_2Cl_2 $\mathbf{13}^+[PF_6]^-$·2CH_2Cl_2, [$Rh_2(PCy_3)${$B(taz)_3$}$_2$][PF_6]$_2$·4CH_2Cl_2 $\mathbf{14}^{2+}$2[PF_6]$^-$·4CH_2Cl_2, and [Rh(PPh_3)I{$B(taz)_3$}] **15** {carried out on Bruker SMART or APEX diffractometers using Mo-Kα X-radiation (λ = 0.71073 Å)} and of [Rh(CO)-{$P(NMe_2)_3$}Tt]·2CH_2Cl_2 **7**·2CH_2Cl_2 and [Rh(CO)(PCy_3)-{$B(taz)_3$}][PF_6]·3CH_2Cl_2 $\mathbf{11}^+[PF_6]^-$·3CH_2Cl_2 {carried out on a Bruker PROTEUM diffractometer using Cu-Kα X-radiation (λ = 1.54178 Å)} are listed in Table 10. The structures of [Rh(CO)(PPh_3)Tt]·CH_2Cl_2 **8**·CH_2Cl_2 (CSD refcode: QEKDAM)

Table 10 Crystal and refinement data for [Rh(cod)Bt] **1**, [Rh(cod)Tt]·0.5H_2O **2**·0.5H_2O, [$(RhTt)_2(\mu\text{-}CO)_3$}] **5**, [Rh(CO)($PCy_3$)Tt]·$CH_2Cl_2$ **6**·CH_2Cl_2, [Rh(CO){$P(NMe_2)_3$}Tt]·2CH_2Cl_2 **7**·2CH_2Cl_2, [Rh{$P(OPh)_3$}$_2$Tt]·1.5CH_2Cl_2 **10**·2CH_2Cl_2, [Rh(CO)(PCy_3){$B(taz)_3$}][PF_6]·3CH_2Cl_2 **11**$^+$[PF_6]$^-$·3CH_2Cl_2, [Rh(CO){$P(NMe_2)_3$}{$B(taz)_3$}][PF_6] **12**$^+$[PF_6]$^-$, [$Rh_2(PCy_3)${$B(taz)_3$}$_2$][PF_6]$_2$·4CH_2Cl_2 **14**$^{2+}$2[PF_6]$^-$·4CH_2Cl_2, [Rh(PPh_3)I{$B(taz)_3$}] **15**

	[Rh(cod)Bt] **1**	[Rh(cod)Tt]·0.5H_2O **2**·0.5H_2O	[$(RhTt)_2(\mu\text{-}CO)_3$}] **5**	[Rh(CO)(PCy_3)Tt]·CH_2Cl_2 **6**·CH_2Cl_2	[Rh(CO){$P(NMe_2)_3$}Tt]·2CH_2Cl_2 **7**·2CH_2Cl_2
Empirical formula	$C_{18}H_{30}BN_6RhS_2$	$C_{46}H_{76}B_2N_{18}ORh_2S_6$	$C_{33}H_{50}B_2N_{18}O_3Rh_2S_6$	$C_{35}H_{60}BCl_2N_9OPRhS_3$	$C_{24}H_{47}BCl_4N_{12}OPRhS_3$
M	508.32	1317.11	1166.71	934.69	902.44
Crystal system	Orthorhombic	Triclinic	Trigonal	Triclinic	Triclinic
Space group	*Pbca*	$P\bar{1}$	$R\bar{3}c$	$P\bar{1}$	$P\bar{1}$
a/Å	12.548(2)	11.263(1)	12.896(2)	11.530(2)	11.697(2)
b/Å	13.774(2)	15.558(1)	12.896(2)	13.237(3)	13.580(3)
c/Å	24.862(3)	17.056(1)	74.468(15)	14.645(3)	14.533(3)
α (°)	90.00	79.575(1)	90.00	87.27(3)	71.41(3)
β (°)	90.00	89.885(1)	90.00	86.12(3)	68.99(3)
γ (°)	90.00	89.542(1)	120.00	79.85(3)	74.88(3)
V/Å^3	4297.1(12)	2939.1(4)	10725(3)	2193.8(8)	2014.4(9)
Z	8	2	6	2	2
μ/mm^{-1}	1.006	0.827	0.674	0.730	8.008
T/K	100	173	100	100	100
Reflections collected	29091	30872	34932	24642	15056
Independent reflections (R_{int})	4925 (0.0485)	13432 (0.0901)	2673 (0.0831)	9963 (0.166)	6792 (0.0623)
Final R indices [$I > 2\sigma(I)$]: $R1$,$wR2$	0.0346, 0.0729	0.0529, 0.1036	0.0501, 0.1543	0.0819, 0.1841	0.0649, 0.1795

	[Rh{$P(OPh)_3$}$_2$Tt]·1.5CH_2Cl_2 **10**·1.5CH_2Cl_2	[Rh(CO)(PCy_3){$B(taz)_3$}][PF_6]·3CH_2Cl_2 **11**$^+$[PF_6]$^-$·3CH_2Cl_2	[Rh(CO){$P(NMe_2)_3$}{$B(taz)_3$}][PF_6] **12**$^+$[PF_6]$^-$	[$Rh_2(PCy_3)${$B(taz)_3$}$_2$][PF_6]$_2$·4CH_2Cl_2 **14**$^{2+}$2[PF_6]$^-$·4CH_2Cl_2	[Rh(PPh_3)I{$B(taz)_3$}]·3CH_2Cl_2 **15**·3CH_2Cl_2
Empirical formula	$C_{105}H_{116}B_2Cl_6N_{18}O_{12}P_4Rh_2S_6$	$C_{37}H_{63}BCl_6F_6N_9OP_2RhS_3$	$C_{22}H_{42}BF_6N_{12}OP_2RhS_3$	$C_{52}H_{89}B_2Cl_8F_{12}N_{18}P_3Rh_2S_6$	$C_{36}H_{45}BCl_6IN_9PRhS_3$
M	2578.54	1248.50	876.52	1990.72	1184.33
Crystal system	Triclinic	Orthorhombic	Triclinic	Triclinic	Monoclinic
Space group	$P\bar{1}$	*Pbca*	$P\bar{1}$	$P\bar{1}$	$P2_1/c$
a/Å	10.309(2)	24.339(5)	11.254(4)	13.412(3)	10.490(1)
b/Å	14.935(3)	15.281(3)	13.158(3)	14.307(3)	20.742(1)
c/Å	19.807(4)	28.840(6)	13.214(13)	24.049(5)	21.960(1)
α (°)	102.89(3)	90.00	113.91(2)	90.85(3)	90.00
β (°)	91.48(3)	90.00	90.92(2)	101.11(3)	92.185(1)
γ (°)	94.73(3)	90.00	95.45(2)	107.75(3)	90.00
V/Å^3	2959.8(10)	10726(4)	1777.5(19)	4299.3(18)	4774.3(3)
Z	1	8	2	2	4
μ/mm^{-1}	0.639	7.508	0.818	0.905	1.543
T/K	173	100	100	100	100
Reflections collected	29160	75672	20527	49319	50648
Independent reflections (R_{int})	29161 (0.0000)	10147 (0.0951)	8130 (0.0223)	19642 (0.0343)	10955 (0.0740)
Final R indices [$I > 2\sigma(I)$]: $R1$,$wR2$	0.1098, 0.2990	0.0523, 0.1432	0.0286, 0.0840	0.0545, 0.1688	0.0473, 0.1089

and [Rh(CO)(PPh_3){$B(taz)_3$}][PF_6]·2CH_2Cl_2 **13**$^+$[PF_6]$^-$·2CH_2Cl_2 (CSD refcode: QEKDEQ) have been published previously.[9]

All data were collected using a CCD area-detector, from a single crystal coated in paraffin oil or high-vacuum grease mounted on a glass fibre. Intensities were integrated[27] from several series of exposures, each exposure covering 0.3° in ω. Absorption corrections were based on equivalent reflections using SADABS,[28] and structures were refined against all F_o^2 data with hydrogen atoms bonded to carbon atoms riding in calculated positions using SHELXTL.[29] The residual electron density map for **5**, **8** and **14**$^{2+}$2[PF_6]$^-$ showed some peaks which could not be modelled satisfactorily; the data for these crystal structures were modelled with PLATON/SQUEEZE.[30] The data completeness for **7** is rather low (89%) due to the difficulties in obtaining a complete sphere of reflections for a triclinic crystal using copper radiation, whilst that for **10** is rather high (213%) due to non-merohedral twinning of the crystal (which also led to high final R values).

Acknowledgements

We thank the EPSRC for postgraduate studentships (to R.J.B., M.F.H. and A.H.), and Johnson Matthey for a generous loan of hydrated rhodium trichloride. We acknowledge the use of the EPSRC's Chemical Database Service at Daresbury.[31]

Notes and references

1 S. Trofimenko, *Scorpionates; The Coordination Chemistry of Polypyrazolylborate Ligands*, Imperial College Press, London, 1999.
2 M. D. Spicer and J. Reglinski, *Eur. J. Inorg. Chem.*, 2009, 1553.
3 M. Careri, L. Elviri, M. Lanfranchi, L. Marchiò, C. Mora and M. A. Pellinghelli, *Inorg. Chem.*, 2003, **42**, 2109.

4 C. E. Webster and M. B. Hall, *Inorg. Chim. Acta*, 2002, **330**, 268.
5 I. R. Crossley, *Adv. Organomet. Chem.*, 2008, **56**, 199.
6 N. G. Connelly, D. J. H. Emslie, W. E. Geiger, O. D. Hayward, E. B. Linehan, A. G. Orpen, M. J. Quayle and P. H. Rieger, *J. Chem. Soc., Dalton Trans.*, 2001, 670.
7 I. R. Crossley, A. F. Hill and A. C. Willis, *Organometallics*, 2006, **25**, 289.
8 V. K. Landry, J. G. Melnick, D. Buccella, K. Pang, J. C. Ulichny and G. Parkin, *Inorg. Chem.*, 2006, **45**, 2588.
9 R. J. Blagg, J. P. H. Charmant, N. G. Connelly, M. F. Haddow and A. G. Orpen, *Chem. Commun.*, 2006, 2350.
10 R. Cammi, M. Lanfranchi, L. Marchiò, C. Mora, C. Paiola and M. A. Pellinghelli, *Inorg. Chem.*, 2003, **42**, 1769.
11 C. A. Tolman, *Chem. Rev.*, 1977, **77**, 313.
12 I. R. Crossley, A. F. Hill, E. R. Humphrey and M. K. Smith, *Organometallics*, 2006, **25**, 2242.
13 B. M. Louie, S. J. Rettig, A. Storr and J. Trotter, *Can. J. Chem.*, 1984, **62**, 633.
14 W. Kläui, M. Scotti, M. Valderrama, S. Rojas, G. M. Sheldrick, P. G. Jones and T. Schroeder, *Angew. Chem., Int. Ed. Engl.*, 1985, **24**, 683.
15 C. J. Adams, K. M. Anderson, J. P. H. Charmant, N. G. Connelly, B. A. Field, A. J. Hallett and M. Horne, *Dalton Trans.*, 2008, 2680.
16 I. R. Crossley, M. R. St-J. Foreman, A. F. Hill, A. J. P. White and D. J. Williams, *Chem. Commun.*, 2005, 221.
17 A. F. Hill, G. R. Owen, A. J. P. White and D. J. Williams, *Angew. Chem., Int. Ed.*, 1999, **38**, 2759.
18 A. G. Orpen, L. Brammer, F. H. Allen, O. Kennard, D. G. Watson and R. Taylor, *J. Chem. Soc., Dalton Trans.*, 1989, S1.
19 N. G. Connelly, N. J. Forrow, B. P. Gracey, S. A. R. Knox and A. G. Orpen, *J. Chem. Soc., Chem. Commun.*, 1985, 14.
20 N. G. Connelly, B. Metz, A. G. Orpen and P. H. Rieger, *Organometallics*, 1996, **15**, 729.
21 I. R. Crossley and A. F. Hill, *Dalton Trans.*, 2008, 201.
22 A. F. Hill, *Organometallics*, 2006, **25**, 4741.
23 G. Parkin, *Organometallics*, 2006, **25**, 4744.
24 M. Sircoglou, S. Bontemps, M. Mercy, N. Saffon, M. Takahashi, G. Bouhadir, L. Maron and D. Bourissou, *Angew. Chem., Int. Ed.*, 2007, **46**, 8583.
25 G. Giordano and R. H. Crabtree, *Inorg. Synth.*, 1990, **28**, 88.
26 N. G. Connelly and W. E. Geiger, *Chem. Rev.*, 1996, **96**, 877.
27 *SAINT integration software*, Bruker AXS, Madison, Wisconsin, 1998–2003.
28 G. M. Sheldrick, *SADABS, Versions 2. 03 (2001) and 2. 10 (2003)*, Bruker AXS, Madison, Wisconsin.
29 G. M. Sheldrick, *Acta Crystallogr., Sect. A: Found. Crystallogr.*, 2008, **64**, 112.
30 A. L. Spek, *Acta Crystallogr., Sect. A: Found. Crystallogr.*, 1990, **46**, C34; A. L. Spek, *PLATON – A Multipurpose Crystallographic Tool*, Utrecht University, Utrecht, The Netherlands, 2006.
31 D. A. Fletcher, R. F. McMeeking and D. Parkin, *J. Chem. Inf. Model.*, 1996, **36**, 746.